Progress In Electromagnetics Research, PIER 26, 67–87, 2000

AN INVERSE SCATTERING APPROACH BASED ON A NEURAL NETWORK TECHNIQUE FOR THE DETECTION OF DIELECTRIC CYLINDERS BURIED IN A LOSSY HALF-SPACE

E. Bermani and S. Caorsi

Department of Electronics
University of Pavia
Via Ferrat 1, I-27100, Pavia, Italy

M. Raffetto

Department of Biophysical and Electronic Engineering
University of Genoa
Via Opera Pia 11A, I-16145, Genoa, Italy

1. INTRODUCTION

The electromagnetic inverse scattering of buried objects represents a topic of growing interest due to the number of applications in seismology, geophysical exploration, ground-penetrating radar and localization of cables and pipes. Generally, in these applications, the detection and/or the dielectric characterization of the target needs to be performed directly "on field". Therefore, the development of an accurate and also fast numerical algorithm for the solution of the inverse scattering problems for buried objects is essential.

In the past years, different approaches, oriented both to a global reconstruction of the internal constitutive parameters [1–7] and to the localization and reconstruction of the external boundary [8–11], have been proposed for the imaging of an object buried in a half-space. In particular, great attention has been devoted to the analysis of cylindrical targets. Chiu and Kiang [8] faced the problem of a conducting cylinder buried in a lossy half-space providing a shape reconstruction. Caorsi *et al.* [2] extended the analysis to dielectric cylinders with a complete characterization of the object. Finally, Qing and Jen [6–7] considered a cylinder embedded in a layered lossless medium. However, even if all these techniques have been proved to provide interesting results, they are, generally, very time consuming.

In this paper, we present a new approach to the inverse scattering problem of buried objects based on the use of a neural network. Overcoming the drawback of directly solving the inverse problem, this technique allows a sensible reduction in the computational time and, consequently, it permits to obtain very fast solutions. Due to this property, it can represent an interesting approach to all those problems requiring an analysis performed directly "on field".

In the following sections the capability of the neural network algorithm to face the inverse scattering problem of buried objects is tested. In particular, the attention is focused on the detection of a given dielectric cylinder located into a well-known half-space scenario. The robustness of the developed technique is also investigated firstly by considering a target and/or an electromagnetic scenario characterized by dielectric parameters different from those used during the training phase and secondly by using noisy input data

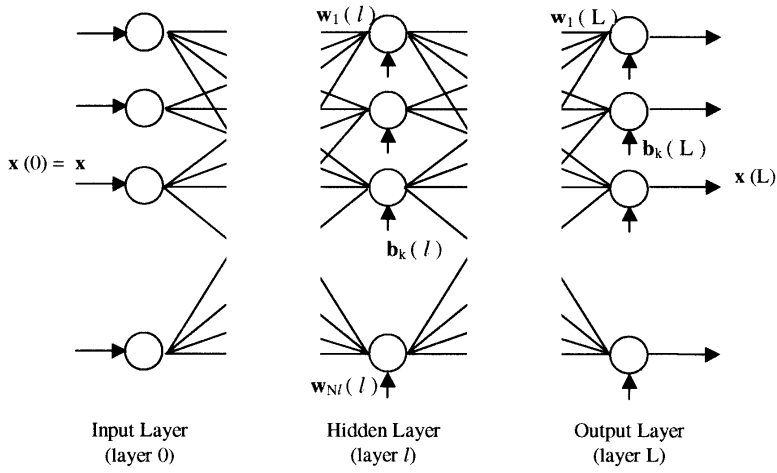

Figure 1. A multi-layer neural network architecture.

2. THE NEURAL NETWORK APPROACH

In this section, the use of a neural network as an inverse scattering technique for the detection of dielectric objects buried in a half-space is outlined. In particular, sub-section 2.1 is devoted to the description of the neural network while the solution of the inverse scattering problems is faced in sub-section 2.2.

2.1 The Neural Network

A neural network is a distributed computational system characterized by a multi-layered structure of neurons fully interconnected via weight links (Fig. 1).

The first layer (input layer or layer 0) is passive: it merely receives the input data from the outside world and sends them to the network. However, in the successive layers (both hidden and output layers), each neuron actively processes, through an appropriate activation function, its input data (Fig. 2). Since each connection is characterized by a weight, the input of every neuron is represented by the weight-output of the previous layer. Each neuron performs a sum of its inputs incremented, usually, with a trainable offset (*bias*) [12]. It means that, if a data pattern $\mathbf{x}$ is applied to the input of the network (see Fig. 1), it propagates through every layer varying the output (*status*) of each

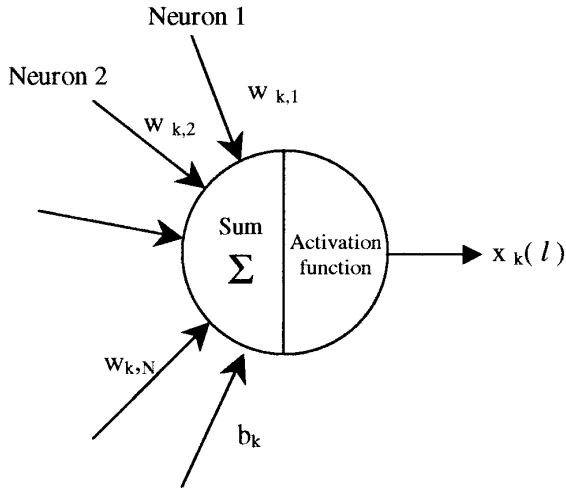

Figure 2. The structure of a neuron of the active (hidden/output) layers.

neuron as follows:

$$x_k(l) = f\left(\sum_{i=1}^{N_1} x_i(l-1)\cdot w_i^{(k)}(l) + b_i(l)\right) \qquad (1)$$
$$\text{for } k = 1\ldots N_l, \quad \text{for } l = 1\ldots L,$$

where: $f(.)$ is the activation function (for instance, a sigmoid);

$x_k(l)$ is the status of the k-neuron of the layer l ;
$w_i^{(k)}$ is the weight associated to the connection between the i-neuron of the layer l -1 and the k-neuron of the layer l ;
$b_k(l)$ is the bias associated to the k-neuron of the layer l
$\mathbf{x}(0) = \{x_1(0)\ldots x_{N_o}(0)\} \equiv \mathbf{x}$ is the input of the neural network
$\mathbf{x}(L)$ is the output of the neural network
N_l and L represent, respectively, the number of neurons in the layer l and the number of active layers.

Therefore the output $\mathbf{x}(L)$ of the neural network can be evaluated as indicated in Figure 3. The values of the weights and bias associated to each layer are defined during the training phase. A set of input patterns characteristic of the investigated problem (training data patterns) is granted to the network and the corresponding output is calculated.

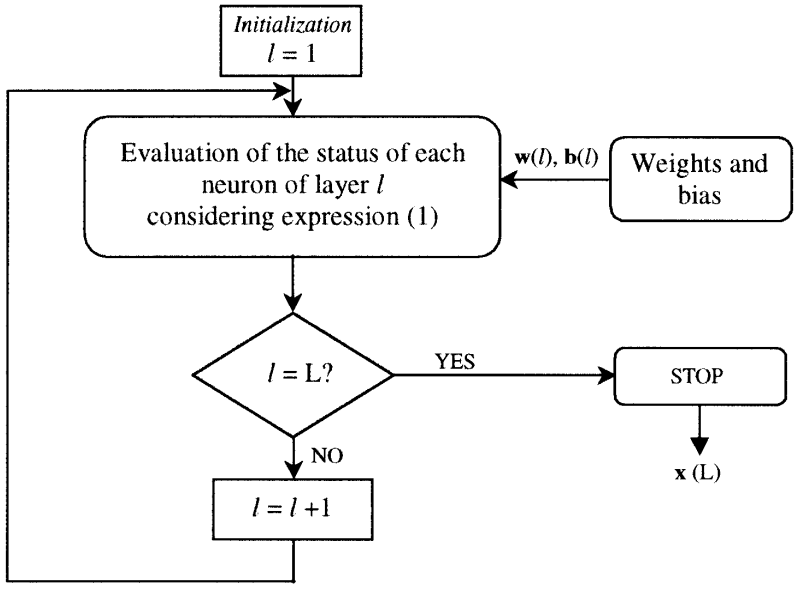

Figure 3. The evaluation of the neural network output (feed-forward phase).

Let us suppose, for instance, that the input data of the training set consist of P patterns $\mathbf{x}^{(p)}, p = 1 \ldots P\}$ and let us assume that $\mathbf{x}^{(p)}(L)$ is the output evaluated by the neural network when the training pattern $\mathbf{x}^{(p)}$ is applied to the input. The total error E of the neural network over the whole training set will be defined as a summation over p of the normalized square difference between $\mathbf{x}^{(p)}(L)$ and the desired output $\mathbf{t}^{p)}$:

$$E = \frac{1}{P \cdot N_L} \sum_{p=1}^{P} \left\| \mathbf{t}^{(p)} - \mathbf{x}^{(p)}(L) \right\|^2 = \frac{1}{P \cdot N_L} \sum_{p=1}^{P} \sum_{k=1}^{N_L} \left\| t_k^{(p)} - x_l^{(p)}(L) \right\|^2 \tag{2}$$

By minimizing, through an appropriate algorithm, the error E with respect to the weights and bias, the strength of each connection can be evaluated and the neural network will be specialized to the solution of a given problem. Therefore, once the training phase is concluded, the neural network can work as a black box system able to provide the solution of a physical problem without directly considering the

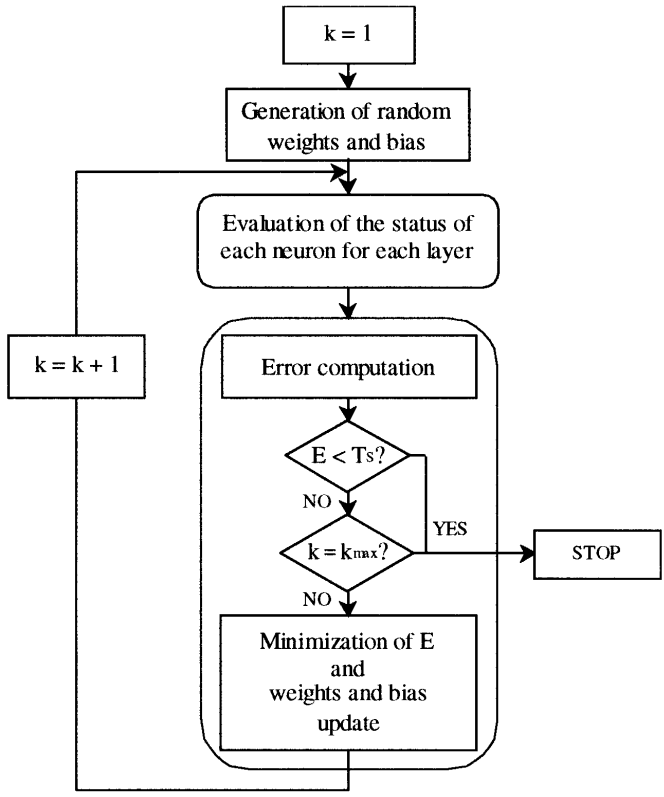

Figure 4. The training algorithm.

functional relation existing between the input and the output values of the problem itself.

In particular, in the detection of dielectric objects buried in a half-space, the use of a neural network, overcoming the drawback of directly solving a complex inverse scattering problem, presents the great advantage of providing a very fast solution to the target-localization problem.

2.1.1 The architecture and the training algorithm

In this work, we have employed a two-layer feed-forword perceptron neural network, with a non constant, bounded and monotone increas-

ing activation function. The capability of this architecture in facing inverse scattering problems has been already shown in the presence of a homogeneous scenario [13]. Therefore, we used it also for the solution of an inverse scattering problem in the presence of a half-space geometry. In particular, we have considered an architecture involving a number of neurons in the hidden layer equal to that of the input layer, as indicated in [13].

The neural network has been trained using a modified version of the Back Propagation code based on the use of the Vogl's acceleration parameter [14, 15]. Figure 4 shows a flowchart of this algorithm. It consists, essentially, of two parts, a feed-forward and a back-propagation phase, that can be described as follows:

Step 0: Generation of random weights and bias:

$\mathbf{w}^{(k)}$ and $\mathbf{b}(l)$ for $k = 1 \dots N_l, l = 1 \dots L$

Step 1: Feed-forward phase:

for each layer $= 1 \dots L$

for each neuron $= 1 \dots N$

$$x_k^{(l)} = f\left(\sum_{i=1}^{N_l} x_i(l-1) \cdot w_i^{(k)}(l) + b_i(l)\right)$$

Step 2: Back-propagation phase:

a) Error computation (as indicated in expression (2))

b) Controls:

If the error E is lower than a fixed threshold $\mathrm{T_S}$

or the maximum number of iterations $\mathrm{k_{max}}$ has been achieved

STOP

c) Minimization of the error and weights/bias update (see [14–15])

d) GOTO **Step 1**

2.2 The Electromagnetic Problem

The problem of the detection of a dielectric buried object is investigated by considering the two-dimensional geometry shown in Figure. 5. The media in regions 1 and 2 are respectively characterized by the complex dielectric permittivity $\varepsilon_1^* = \varepsilon_0[\varepsilon_{r1} - j\sigma_1/\omega\varepsilon_0]$ and

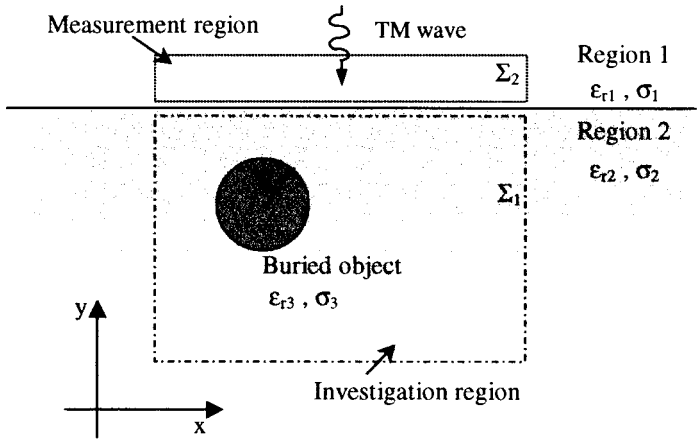

Figure 5. The geometry of the problem.

$\varepsilon_2^* = \varepsilon_0[\varepsilon_{r2} - j\sigma_2/\omega\varepsilon_0]$ while the magnetic permeability is that of the vacuum in each region.

Let $\sum_1$ represent the investigation domain where the target can be located and let $\sum_2$ be the measurement region. The position of the cylinder represents the unknown of the problem while its complex dielectric permittivity is given by $\varepsilon_3^* = \varepsilon_0[\varepsilon_{r3} - j\sigma_3/\omega\varepsilon_0]$. A TM-wave incident field is used as illuminating source.

The problem described above is generally faced starting from the integral formulation of the electromagnetic scattering. As a consequence, the location of the object is performed solving a complex non linear problem. However, by introducing some *a priori* information the number of the unknowns can be greatly reduced. This information can be obtained, for instance, focusing the attention on cylindrical targets of a given circular section. In particular, the localization of the target can be performed considering as unknown variables the coordinates of the center of the cylinder section in the xy plane (x_C and y_C) The position of the cylinder will represent the output of the neural network while the inputs are given by the complex values of the electric scattered field measured at a number of points near the interface between the two media (Fig. 5).

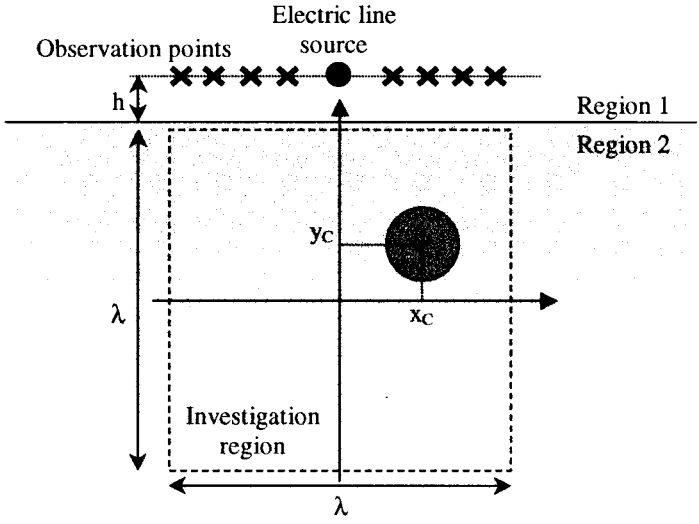

Figure 6. The physical system under investigation: a circular cylinder of unknown position is located in a square investigation region and illuminated by an electric line source operating at a frequency equal to 500 MHz.

3. NUMERICAL RESULTS

Let us consider the geometrical configuration shown in Figure 6. An electric line source, located in the region 1 and parallel to the axis of the cylinder (i.e. parallel to the z-axis), is supposed to illuminate a square investigation domain having a side of length λ, where λ represents the wavelength in free space. Sixteen equally spaced observation points are arranged in region 1 along a probing line near the interface between the two media ($h = \lambda/6$).

An electromagnetic scenario characterized by dielectric parameters $\varepsilon_{r1} = 1.0$ and $\sigma_1 = 0.0$ in region 1 and $\sigma_{r2} = 20.0$ and $\varepsilon_2 = 0.01$ in region 2 is considered for our analysis. Moreover, we assume that the buried object is a circular cylinder of radius equal to $\lambda/12$ and dielectric characteristics given by $\varepsilon_{r3} = 5.0$ and $\sigma_3 = 0.0$.

The data used to generate the training set and those considered to test the neural network have been obtained by employing a Finite Element code and a PML technique [16, 17]. In particular, 700 examples, obtained by moving the cylinder described above in the investigation domain, have been considered during the learning phase.

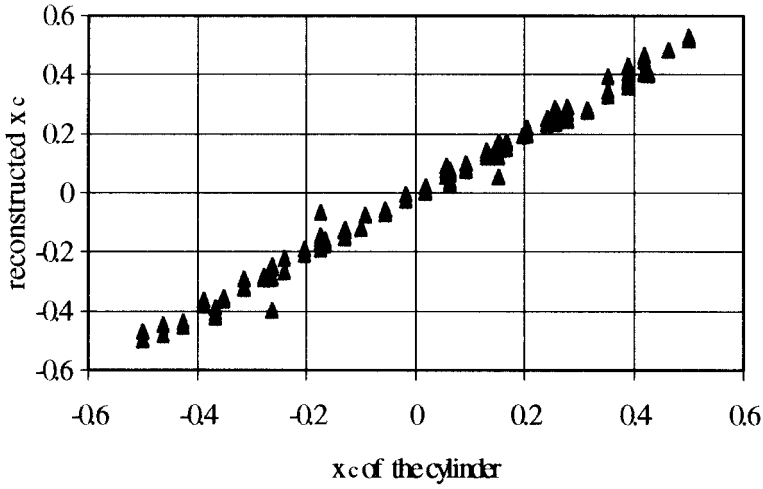

(a)

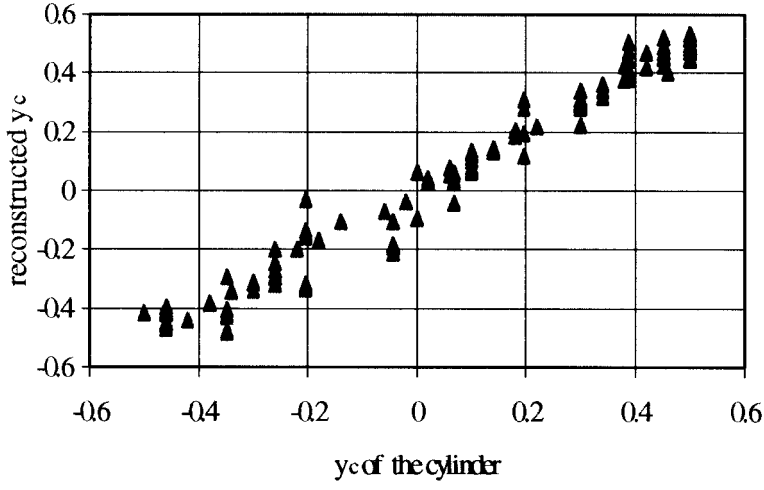

(b)

Figure 7. The reconstructed coordinates x_C (a) and y_C (b) of the center of the cylinder versus the actual ones for a test set of 160 examples. A scale normalized to λ is considered on both axes.

3.1 Validation of the Neural Network Technique

In the first set of simulations, the capability of the neural network to detect the dielectric cylinder is tested for different location of the target inside the investigation region: in particular, 160 positions, equally distributed in the investigation domain, have been taken into account. Figure 7 shows the results of the localization for the examples making up the test set. As can be seen, a good accuracy in the localization is achieved along both the x- and the y-axis (Tab. 1). In particular, we observe that, even if the accuracy in the detection is lower when the distance from the interface between regions 1 and 2 is bigger, good results are obtained in the whole domain with a medium error ranging between 0.021 and 0.039λ for x_C and between 0.021 and 0.072λ for y_C .

Range	**Medium error**	**Maximum error**
$0.0 < \|x_C\| < 0.1$	0.021	0.041
$0.1 < \|x_C\| < 0.2$	0.023	0.132
$0.2 < \|x_C\| < 0.3$	0.030	0.230
$0.3 < \|x_C\| < 0.4$	0.032	0.083
$0.4 < \|x_C\| < 0.5$	0.039	0.081

Table 1. Medium and maximum errors in the reconstruction of x_C for a test set of 160 examples. The errors are normalized to λ.

Range	**Medium error**	**Maximum error**
$-0.5 < y_C\| < 0.4$	0.045	0.091
$-0.4 < y_C\| < 0.3$	0.072	0.136
$-0.3 < y_C\| < 0.2$	0.071	0.171
$-0.2 < y_C\| < 0.1$	0.037	0.092
$-0.1 < y_C\| < 0.0$	0.068	0.160
$0.0 < y_C\| < 0.1$	0.032	0.110
$0.1 < y_C\| < 0.2$	0.021	0.062
$0.2 < y_C\| < 0.3$	0.039	0.110
$0.3 < y_C\| < 0.4$	0.038	0.102
$0.4 < y_C\| < 0.5$	0.036	0.093

Table 2. Medium and maximum errors in the reconstruction of y_C for a test set of 160 examples. The errors are normalized to λ.

3.2 Robustness of the Network

In the second set of simulations we tested the robustness of the neural network firstly by using problem configurations different from those considered to generate the training set and secondly by considering noisy input data patterns. In particular, the effects of some variations in the dielectric properties of both the cylinder and the electromagnetic scenario and the robustness of the developed neural network to input data affected by a white noise have been taken into account.

3.2.1 Variations in the dielectric properties of the cylinder

This analysis has been performed in three different steps. Firstly, we considered a variation of the relative dielectric permittivity of the target. Then, we investigated the effects of a variation in its conductivity and, in particular, the consequences due to the presence in the observation domain of the lossy cylinder instead of the lossless one, such that used during the training phase. Finally, we supposed that both the dielectric parameters could change. For all simulations of the direct scattering problem, the cylinder is supposed to be located at a dept of 0.5 λ. For simplicity we assumed such a position as a reference point ($x_C = 0$ and $y_C = 0$)

Figure 8 shows the results of the localization for cylinders characterized by a relative dielectric permittivity varying in the range $[\,4.5 \div 5.5\,]$ (i.e., $\varepsilon_{r3} \pm 10\%$). The error is lower than 0.006 λ for x_C and inferior to 0.035 λ for y_C - The same results have been obtained for a lossy cylinder having a conductivity ranging between 10^{-5} S/m and 10^{-2} S/m (fig. 9). In particular, in this last case it is important to observe that the developed neural network, trained considering only lossless cylinders, allows to detect also lossy cylinders.

Finally, we extended the previous analysis considering the case of a cylinder whose dielectric characteristics changed simultaneously. In particular, we assumed that the relative dielectric permittivity varied in the range $[\,4.8 \div 5.2\,]$ while the conductivity could change between 10^{-5} S/m and 10^{-2} S/m. Also in this case, the localization is performed with a good accuracy. The errors in the detection remained lower than 0.006 λ for x_C and inferior to 0.05 λ for y_C (fig. 10).

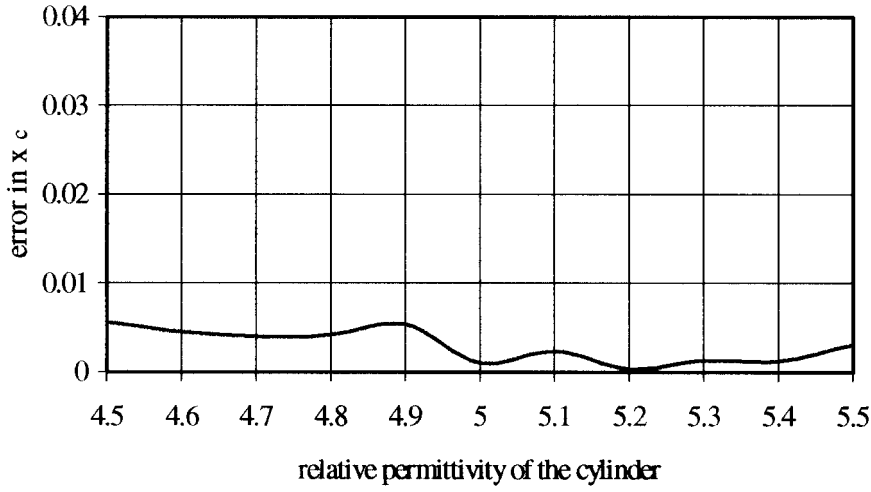

(a)

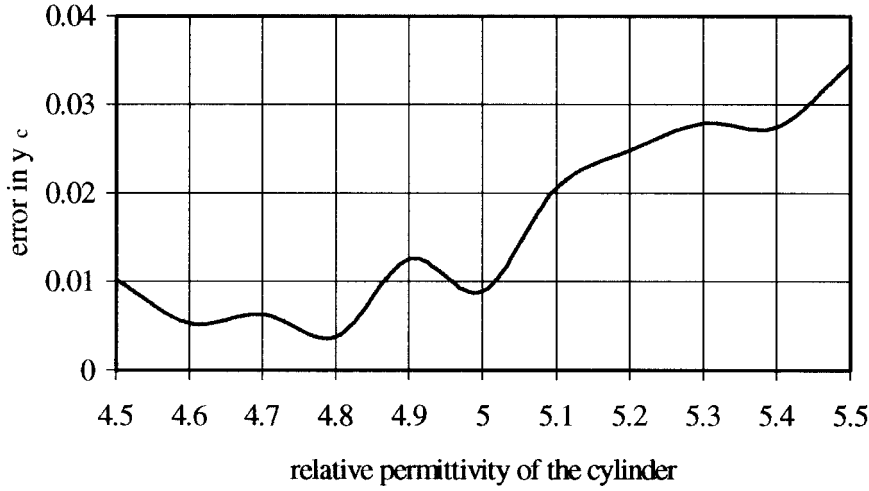

(b)

Figure 8. The medium errors in the reconstruction of x_C (a) and y_C (b) for cylinders characterized by $\varepsilon_{r3} = \tilde{\varepsilon}_r \pm 10\%$, where $\tilde{\varepsilon}_r$ is the relative dielectric permittivity considered during the training phase (i.e., $\tilde{\varepsilon}_r = 5$). The error values are normalized to λ.

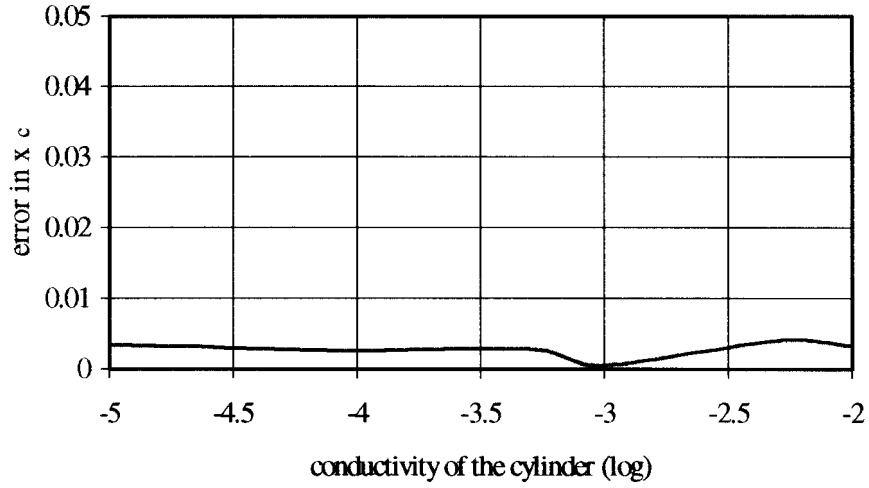

(a)

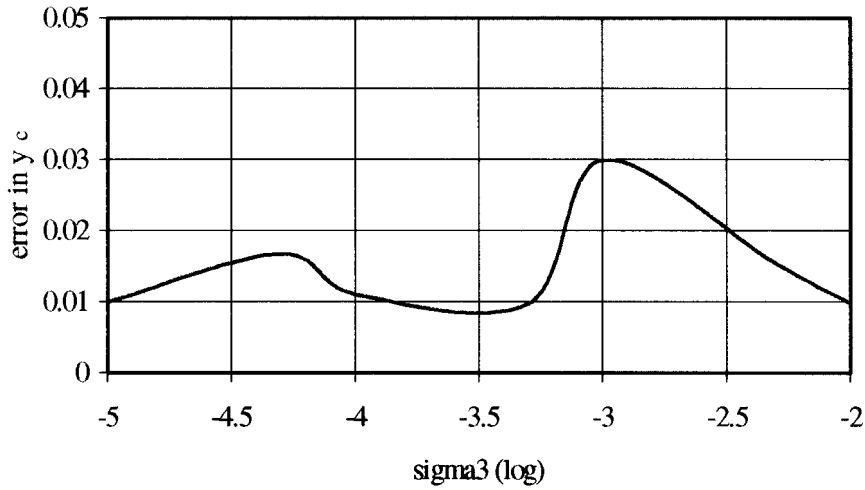

(b)

Figure 9. The medium errors in the reconstruction of x_C (a) and y_C (b) for cylinders characterized by values of the conductivity varying in the range $[10^{-5} \div 10^{-2}]$. A logrithmic scale is used on the conductivity-axis. The values of the error are normalized to λ.

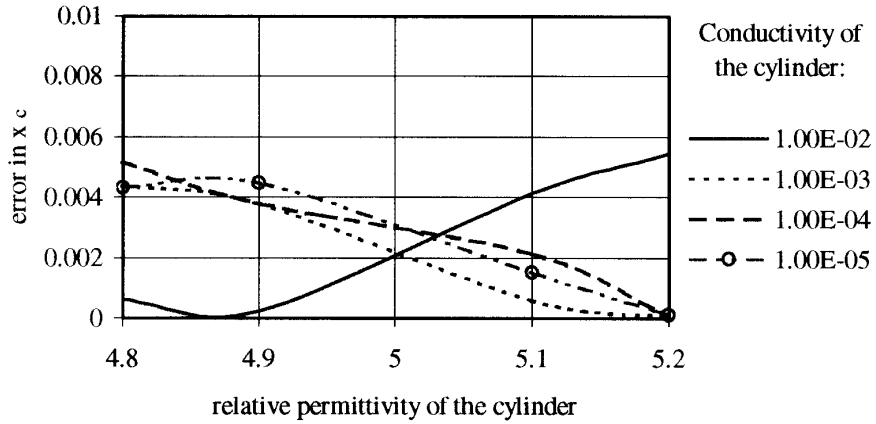

(a)

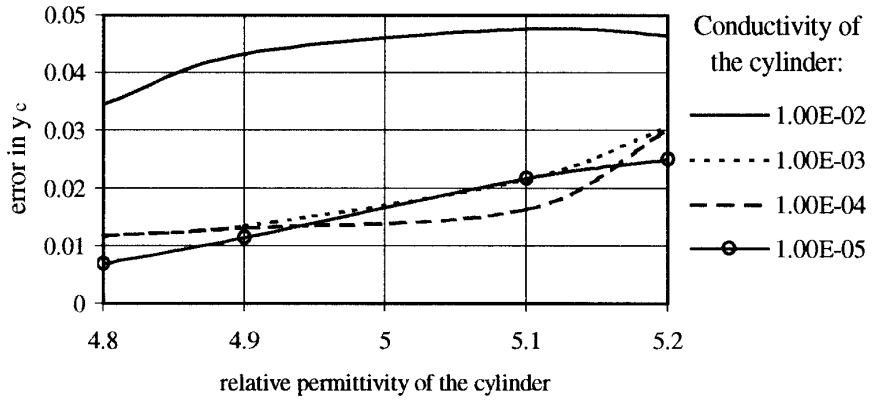

(b)

Figure 10. The medium errors in the reconstruction of x_C (a) and y_C (b) for cylinders characterized by $\varepsilon_{r3} = \tilde{\varepsilon}_r \pm 4\%$, where $\tilde{\varepsilon}_r$ is the relative dielectric permittivity considered for the clyinder during the training phase (i.e., $\tilde{\varepsilon}_r = 5$), and values of the conductivity varying in the range $[10^{-5} \div 10^{-2}]$. The error values are normalized to λ.

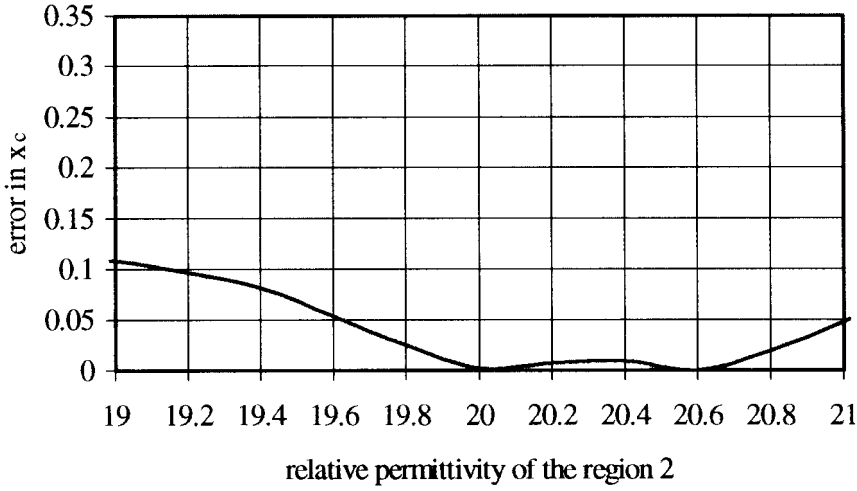

(a)

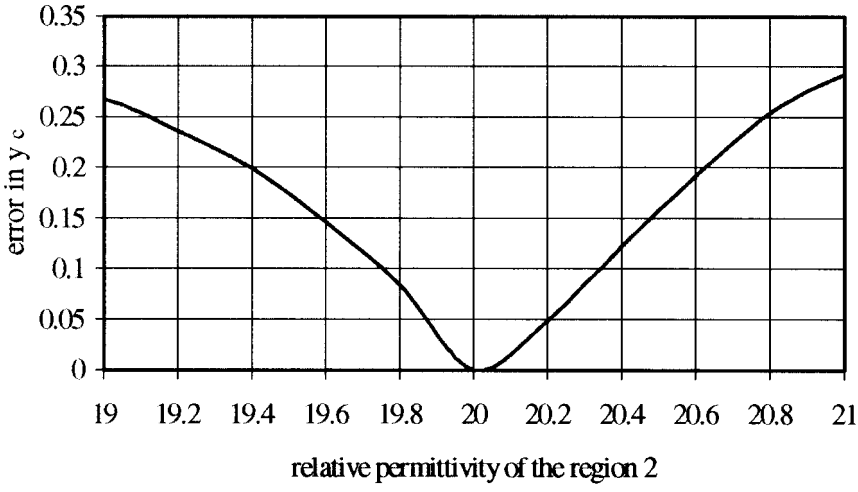

(b)

Figure 11. The medium errors in the reconstruction of x_C (a) and y_C (b) when region 2 is characterized by $\varepsilon_{r2} = \tilde{\varepsilon}_r \pm 5\%$, where $\tilde{\varepsilon}_r$ is the relative dielectric permittivity used during the training phase (i.e., $\tilde{\varepsilon}_r = 20.0$). The error values are normalized to λ.

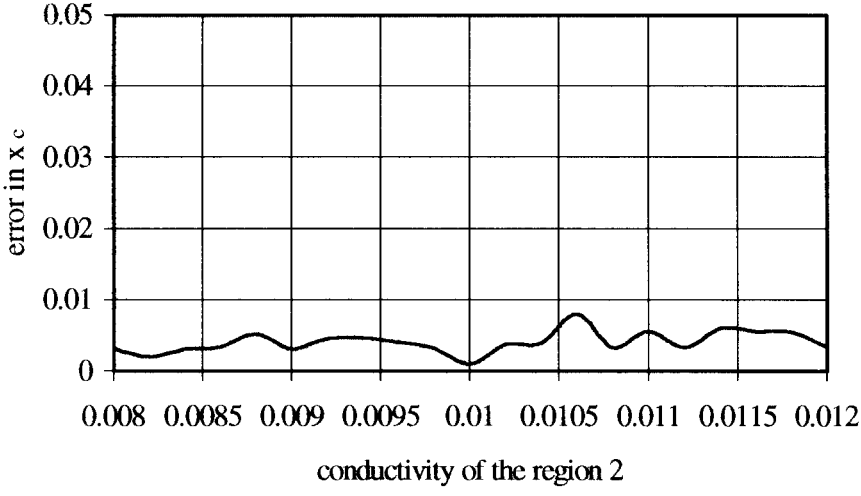

(a)

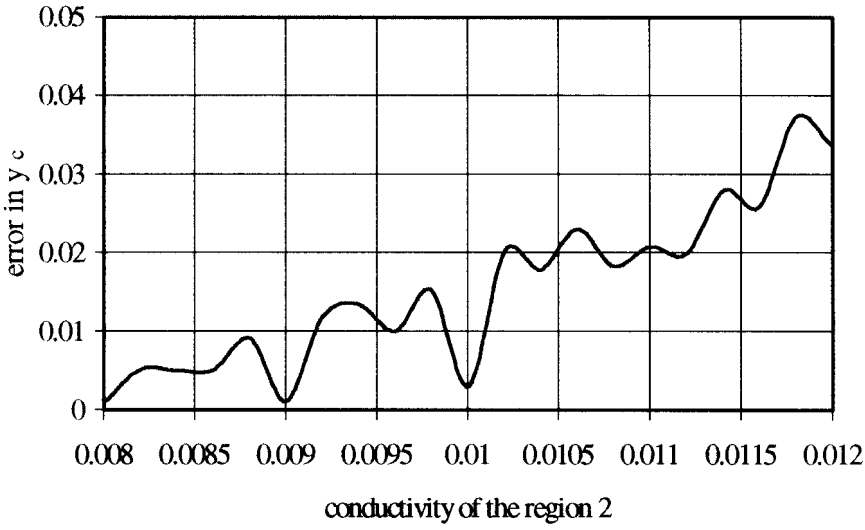

(b)

Figure 12. The medium errors in the reconstruction of x_C (a) and y_C (b) when region 2 is characterized by $\sigma_3 = \tilde{\sigma} \pm 20\%$, where $\tilde{\sigma}$ indicated the conductivity used during the training phase (i.e., $\tilde{\varepsilon}_r = 5$). A logrithmic scale is used for the conductivity. The error values are normalized to λ.

3.2.2 Variations in the dielectric properties of the scenario

As a second test, we considered a variation in the dielectric properties of the electromagnetic scenario. The effects due to a change in both the relative dielectric permittivity and the conductivity of the medium in region 2 have been taken into account and treated separately. In particular, we have examined firstly a variation of the relative dielectric permittivity in the range $[\,19 \div 21\,]$ (i.e., $\varepsilon_{r2} \pm 10\%$); then, we investigate the effects of a conductivity ranging between 0.008 S/m and 0.012 S/m (i.e., $(\,\sigma_2 \pm 20\%\,)$.

Figures 11 and 12 show the errors in the localization of the cylinder having the same characteristics as that considered for the training phase ($\varepsilon_{rs} = 5.0$ and $\sigma_3 = 0.0$). The cylinder is assumed to be located at the reference position $x_C = 0$ and $y_C = 0$. We observe that, while a variation in the conductivity of the medium has a little influence in the detection of the target (x_C and y_C are reconstructed with errors less than 0.009 and 0.037 λ, respectively), the relative dielectric permittivity represents, as expected, a more delicate parameter. In particular, only little variations are allowed to obtain a limited error. This is verified especially for the reconstruction of the y- coordinate of the cylinder center.

3.2.3 Robustness to noisy data

In order to test the robustness of the developed technique in the presence of noisy input data, we considered the localization of the cylinder for different signal-to-noise ratio. In particular, we assumed that a white noise affected the input values of the neural network (i.e., the values of the scattered electric field). Three different positions of the target have been taken into account. For all the simulations, the buried cylinder and the electromagnetic scenario are supposed to be characterized by the same dielectric properties considered during the training phase.

Figure 13 shows where the neural network localized the object, respectively, $x_C = -0.28\ \lambda$ and $y_C = 0.38\ \lambda$ (case a), $x_C = 0.33\ \lambda$ and $y_C = 0.3\ \lambda$ (case b), $x_C = 0.0\lambda$ and $y_C = -0.42\ \lambda$ (case c). The errors in the localization are reported in Tab. 3. As can be seen, the localization of the cylinder is achieved with a good accuracy also in the presence of noisy input data.

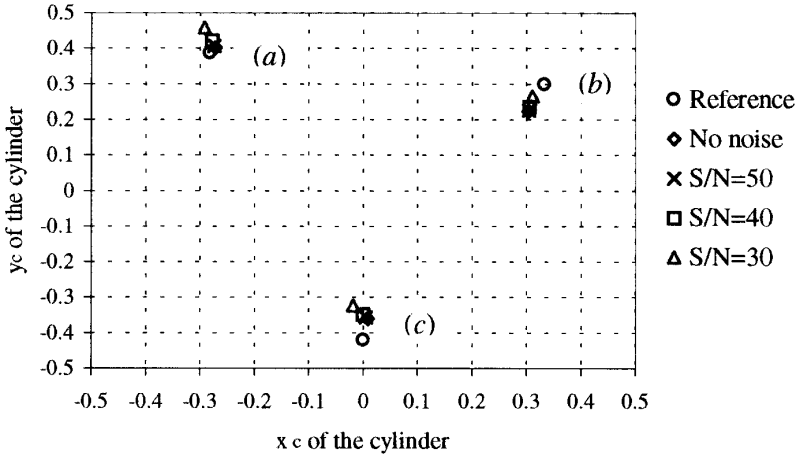

Figure 13. Reconstruction of the position of the center of the cylinder for different signal-to-noise ratios when, respectively, $x_C = -0.28\ \lambda$ and $y_C = 0.38\ \lambda$ (case a), $x_C = 0.33\ \lambda$ and $y_C = 0.3\ \lambda$ (case b), $x_C = 0.0\lambda$ and $y_C = -0.42\ \lambda$ (case c).

Test	Coordinate	No noise	S/N = 50	S/N = 40	S/N = 30
a	x_C	0.009	0.007	0.003	0.011
a	y_C	0.013	0.020	0.034	0.060
b	x_C	0.020	0.030	0.027	0.023
b	y_C	0.050	0.051	0.046	0.039
c	x_C	0.007	0.005	0.005	0.019
c	y_C	0.050	0.051	0.070	0.081

Table 3. Errors in the reconstruction of x_C and y_C for different signal-to-noise ratios when respectively, $x_C = -0.28\lambda$ and $y_C = 0.38\lambda\ (a)$, $x_C = 0.33\lambda$ and $y_C = 0.3\lambda\ (b)$, $x_C = 0.0\lambda$ and $y_C = -0.42\lambda\ (c)$,

4. CONCLUSION

A neural network approach to the detection of two-dimensional dielectric cylinders buried in a lossy half-space geometry has been proposed. The results obtained seem to be very interesting. The developed neural network technique has been proved to localize not only targets with

the same dielectric properties used for the training set but also objects characterized by a dielectric permittivity different up to 10% from that considered during the learning phase. Moreover, we showed that lossy dielectric cylinders can be detected by using a neural network trained by considering only lossless cylinders. Then, as far as possible variations in the electromagnetic scenario are concerned, we proved that this technique can be adopted to localize object buried into an investigation domain characterized by a conductivity different up to 20% from that of the training set examples. This result can be very interesting, in particular for possible applications of the neural network technique to situations where the conductivity of the scenario can change in a big range of value (for instance, between dry or wet soil). Finally, also the robustness to noisy input data has been shown.

REFERENCES

1. Chammeloux, L., C. Pichot, and J. C. Bolomey, "Electromagnetic modeling for microwave imaging of cylindrical buried inhomogeneities," *IEEE Trans. Microwave Theory Tech,* Vol. 34, No. 10, 1064–1076, 1986.
2. Caorsi, S., G. L. Gragnani, and M. Pastorino, "Numerical electromagnetic inverse-scattering solutions for two dimensional infinite dielectric cylinders buried in a lossy half-space," *IEEE Trans. on Microwave Theory and Tech.,* Vol. MTT-41, 352–356, 1993.
3. Akduman, I., "An inverse scattering problem related to buried cylindrical bodies illuminated by Gaussian beams," *Inverse Problems,* Vol. 10, 213–226, 1994.
4. Chaturvedi, P., and R. G. Plumb, "Electromagnetic imaging of underground targets using constrained optimization," *IEEE Trans. on Geoscience and Remote Sensing,* Vol. 33, 551–561, 1995.
5. Chiu, C.-C., and C.-P. Huang, "Inverse scattering of dielectric cylinders buried in a half-space," *Microwave and Optical Tech. Lett.,* Vol. 13, 96–99, 1996.
6. Qing, A., and L. Jen, "Microwave imaging of dielectric cylinder in a layered media," *Journal of Electromagnetic Waves and Applications,* Vol. 11, 259–269, 1997.
7. Qing, A., and L. Jen, "A novel method for microwave imaging of dielectric cylinder in layered media," *Journal of Electromagnetic Wavesand Applications,* Vol. 11, 1337–1348, 1997.

8. Chiu, C.-C., and Y.-W. Kiang, "Electromagnetic inverse scattering of a conducting cylinder buried in a lossy half-space," *Trans. on Antennas and Propagation,* Vol. AP-40, 1562–1564, 1992.
9. Osumi, N., and K. Ueno, "Microwave holographic imaging of underground objects," *Trans. on Antennas and Propagation,* Vol. AP-33, 152–159, 1985.
10. Iizuka, K., and A. Freundofer, "Detection of nonmetallic buried objects by a step-frequency radar," *Proc. IEEE,* Vol. 71, 276–279, 1983.
11. Chen, L. C., D. L. Muffatt, and L. Peters, "Improved performance of a subsurface radar target identification system through antenna design," *IEEE Trans. on Antennas and Propagation,* Vol. AP-29, 307–311, 1981.
12. Dayhoff, J. E., *Neural Network Architectures: an introduction,* New York: Van Nostrand, 1990.
13. Caorsi, S., and P. Gamba, "Electromagnetic detection of dielectric cylinder by a neural network approach," *IEEE Trans. on Geoscience and Remote Sensing,* Vol. 37, 820–827, 1999.
14. Rumelhart, D. E., G. E. Hinton, and R. H. Williams, "Learning representation by backpropagating errors," *Nature,* Vol. 323, 533–536, 1986.
15. Vogl, T. P., J. K. Mangis, A. K. Rigler, W. T. Zink, and D. L. Aljkon, "Accelerating the convergence of the back-propagation method," *Biol. Cybern.,* Vol. 59, 257–263, 1988.
16. Sacks, Z. S., D. M. Kingsland, R. Lee, and J.-F. Lee, "A perfectly matched anisotropic absorber for use as an absorbing boundary condition," *IEEE Trans. on Antennas and Propagation,* Vol. AP-43, 1460–1463, 1995.
17. Caorsi, S., and M. Raffetto, "Perfectly Matched Layer for the truncation of the finite element meshes in layered half-space geometries and applications to the electromagnetic scattering by buried objects," *Microwave and Optical Tech. Lett.,* Vol. 19, 427–434, 1998.